Impact of pentacene film thickness on the photoresponse spectra: Determination of the photocarrier generation mechanism

S. Gorgolis, A. Giannopoulou, D. Anastassopoulos, and P. Kounavis

Citation: Journal of Applied Physics **112**, 013101 (2012); doi: 10.1063/1.4730915
View online: http://dx.doi.org/10.1063/1.4730915
View Table of Contents: http://scitation.aip.org/content/aip/journal/jap/112/1?ver=pdfcov
Published by the AIP Publishing

Impact of pentacene film thickness on the photoresponse spectra: Determination of the photocarrier generation mechanism

S. Gorgolis,[1] A. Giannopoulou,[1] D. Anastassopoulos,[2] and P. Kounavis[1,a)]
[1]*Department of Engineering Sciences, University of Patras, 26504 Patra, Greece*
[2]*Department of Physics, University of Patras, 26504 Patra, Greece*

(Received 2 March 2012; accepted 27 May 2012; published online 2 July 2012)

Photocurrent response, optical absorption, and x-ray diffraction (XRD) measurements in pentacene films grown on glass substrates are performed in order to obtain an insight into the mobile photocarriers generation mechanism. For film thickness of the order of 50 nm and lower, the photocurrent response spectra are found to follow the optical absorption spectra demonstrating the so-called symbatic response. Upon increasing the film thickness, the photoresponse demonstrates a transition to the so-called antibatic response, which is characterized by a maximum and minimum photocurrent for photon energies of minimum and maximum optical absorption, respectively. The experimental results are not in accordance with the model of important surface recombination rate. By taking into account the XRD patterns, the experimental photoresponse spectra can be reproduced by model simulations assuming efficient exciton dissociation at a narrow layer of the order of 20 nm near the pentacene-substrate interface. The simulated spectra are found sensitive to the film thickness, the absolute optical absorption coefficient, and the diffusion exciton length. By comparing the experimental with the simulated spectra, it is deduced that the excitons, which are created by optical excitation in the spectral region of 1.7-2.2 eV, diffuse with a diffusion length of the order of 10-80 nm to the pentacene-substrate interface where efficiently dissociate into mobile charge carriers. [http://dx.doi.org/10.1063/1.4730915]

I. INTRODUCTION

Organic semiconductors have received a considerable attention due to their peculiar electronic transport and photoelectronic properties making them very attractive for many low cost technological applications.[1–5] Among the organic semiconductors, pentacene has been intensively studied.[6] A considerable progress has been achieved in the fabrication procedure and a high mobility material was obtained.[7–10] This development opened the field to develop high performance organic thin film transistors (OTFTs) based on pentacene which compete the respective devices based on amorphous silicon.[11] Moreover, pentacene due to its improved transport properties together with its high photosensitivity makes it an appropriate material in many potential optoelectronic applications, such as photodectors,[12] solar cells,[13,14] and sensors.[15] The performance of such devices is governed by the trapping of carriers at various interfaces and at the grain boundaries in the polycrystalline pentacene film.[16,17] Furthermore, hysteresis phenomena in these devices have been attributed to trapping of carriers and various studies have been devoted to explore further this effect. Besides this, the photocarrier generation mechanism is essential in the design of optoelectronic devices. However, the details of this mechanism are poorly understood and need further investigation.

Various optical transitions have been observed in pentacene films within the spectral region of 1.7–2.8 eV, without a common interpretation. In organic semiconductors, mobile charge carrier creation may take place not only by interband optical transitions across the higher occupied molecular orbit (HOMO) to lower unoccupied molecular orbit (LUMO) but also by an extrinsic process. The extrinsic process involves creation by light of excitons which may dissociate into mobile charge carriers. These excitons have been earlier identified as Frenkel and charge transfer excitons.[18] However, the nature of the excitons as well as the charge separation remain unclear and various optical spectroscopic studies have been dedicated to shed light on this issue.[19,20] The spectral response of the photocurrent has been employed to study the energy distribution of the excited states of organic semiconductors, the charge carrier creation mechanism, and the identification of the optical transitions.[21–25] Nevertheless, the presence of different optical transitions within a limited energy region complicates their identification and the determination of the exact HOMO-LUMO gap of pentacene. Various optical absorption studies on pentacene films reported completely different gap energies ranging between 1.7 eV and 2.8 eV.[18,26–29]

In this work, optical absorption from transmission-reflection measurements in the spectral region of 1.7–2.8 eV is employed to determine the main optical transitions of pentacene films on glass substrate. A direct comparison of the features observed in the optical absorption spectra with those observed in the photocurrent response spectra of samples with top gold coplanar contacts are systematically studied. From this comparison, the optical transitions which lead to charge carrier creation are identified. By illuminating the pentacene films of different thickness with exciting light of different penetration depths, the effective region of the films participating in the photocurrent generation is determined.

a)Electronic address: pkounavis@des.upatras.gr.

The experimental results are modelled by employing different possible photogeneration processes, in order to obtain an insight into the charge carrier creation mechanism and to specify the basic parameters governing the photoresponse spectra. The appropriate mechanism of mobile charge carrier creation which satisfactorily reproduces the experimental spectra and at the same time is compatible with the x-ray diffraction (XRD) measurements is concluded.

II. DETAILS OF SAMPLE FABRICATION AND CHARACTERIZATION

A vacuum chamber with a turbo molecular pump and a mechanical rotary pump for backing were used to deposit pentacene films. A base vacuum of $1-2\times10^{-6}$ Torr was reached before deposition. The deposition rate and the film thickness during deposition were monitored by means of a quartz-crystal microbalance. The pentacene was purchased from Sigma Aldrich (97% purity) and was used without further purification. Prior the deposition, the pentacene was degassed holding the evaporation source at a temperature slightly lower than the sublimation temperature of pentacene. For this purpose, a shutter covers the substrates, leaving only the quartz crystal exposed to the evaporation source in order to confirm negligible pentacene evaporation. In this way, unintentional volatile impurities from the fabrication process of pentacene are removed, whereas impurities with low volatility remain on the evaporation source.[30] Subsequently, the deposition rate was stabilized to the desired value for a few minutes before the onset of the deposition and then the shutter was removed in order to deposit pentacene films on 7059 corning glass substrates. The deposition rate was 0.13 Å/s for the thinner films and increased up to 1.3 Å/s for the thicker films, so approximately the same total deposition time of about 1 h was obtained for all the samples. This way, longer deposition times, which may enhance the probability of contamination of the thicker films by unintentional impurities during pentacene evaporation, are avoided. The pentacene films had different nominal thicknesses, d, covering the region from 18 nm to 357 nm. After film deposition, the vacuum was break for a few minutes, in order to insert the mask and to deposit two coplanar gold electrodes on the top of the pentacene having 6 mm length separated by a gap of 450 μm. The electrodes had a thickness of 50 nm and were deposited under a vacuum of $3-4\times10^{-6}$ Torr with a stabilized deposition rate of 3 Å/s.

The optical properties of the pentacene films were characterized by optical transmission and reflection measurements in the ambient air from which the optical absorption coefficient, α, was calculated. For this purpose, the light from a 100 W tungsten-halogen lamp was passed through a monochromator, appropriate filters, a mechanical chopper of frequency of 273 Hz and focused on the sample. The transmitted and reflected light beams were measured by a silicon detector.

For the photoelectric properties characterization, the sample was transferred in an optical cryostat with a base vacuum of 3×10^{-3} Torr. The light from the monochromator was mechanically chopped at the frequency of 12 Hz and focused on the sample in the cryostat. The resulting photocurrent was amplified and measured using phase-sensitive detection. For this purpose, a digital lock-in amplifier **(Stanford Research Systems SR830)** was used, while the chopper signal was used as the reference signal. The absolute incident photon flux, F_0, was measured by a calibrated silicon diode **(Newport 918D-UV-OD3)** placed at the site of the sample.

The structure of the pentacene films with different thickness were characterized by XRD measurements in the symmetric reflection coupled $\theta-2\theta$ arrangement. The XRD patterns were obtained using $CuK\alpha$ radiation.

III. RESULTS

A. Optical properties

Fig. 1 presents the optical absorption coefficient α as a function of photon energy of pentacene films having the indicated thickness. As a general trend, the overall absolute optical absorption coefficient values in the entire photon energy region appear relatively lower in thicker samples compared to those of the thinner films. Four absorption bands peaked at about $E_A=1.80-1.85$ eV, $E_B=1.94-1.97$ eV, $E_C=2.11-2.13$ eV, and $E_D=2.26-2.28$ eV are observed which are typical for pentacene films.[31] Fig. 2 presents the peak energies of the above absorption bands as a function of d. The two maxima at the lower photon energies E_A and E_B are usually attributed to the Davydov doublet due to singlet exciton absorption.[32,33] The two other maxima at the higher photon energies E_C and E_D are usually attributed to charge-transfer excitons.[18] It is worth mentioning the small broad shoulder, which systematically appears around $E_G\cong2.4$–2.6 eV in the absorption spectra for all the samples of Fig. 1. This feature is

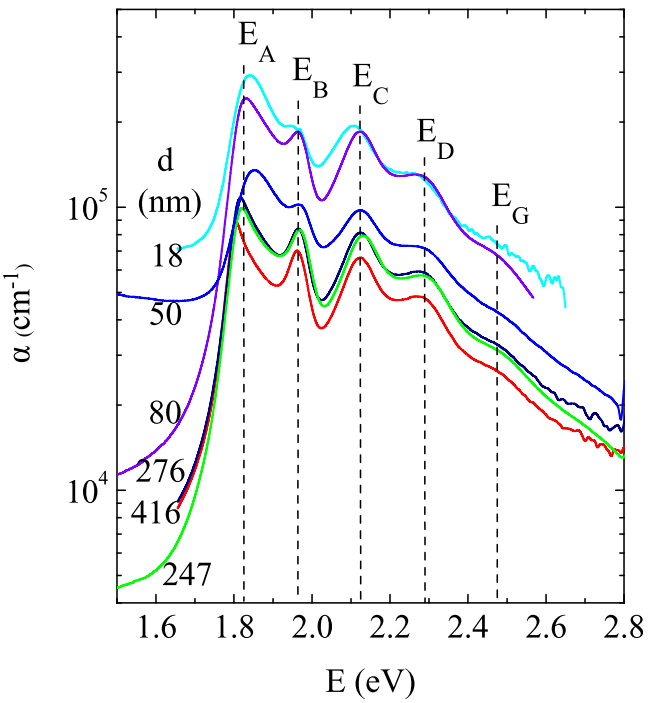

FIG. 1. Optical absorption coefficient spectra of pentacene films with the indicated thickness, d. E_A, E_B, E_C, and E_D denote the peak energies of the main absorption bands. E_G denotes a shoulder in the spectra around 2.4–2.6 eV.

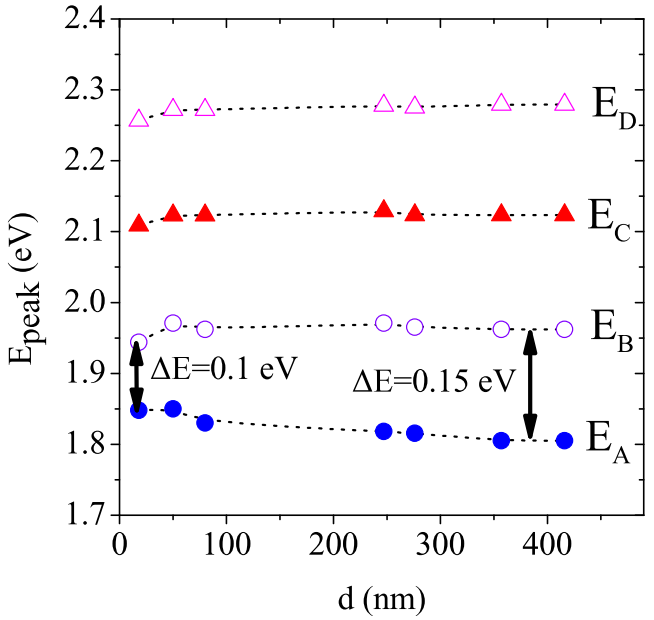

FIG. 2. Evolution with the thickness d of the peak energies E_A, E_B, E_C, and E_D of the main absorption bands of the optical absorption spectra. ΔE denotes the Davidov splitting of the low energy peaks at E_A and E_B. Dashed lines serve as guide lines.

also found in most of absorption spectra reported in the literature.

The splitting ΔE, defined as $\Delta E = E_B - E_A$, of the Davydov doublet is a measure of the strength of the interatomic forces. ΔE is found to decrease from about 0.15 eV to 0.1 eV with decreasing the film thickness (see Fig. 2), in very good agreement with the results of the literature.[34] The decrease of ΔE predominantly takes place in films thinner than 80 nm and arises from a blue and red shift of the peaks at E_A and E_B, respectively. Based on this observation, it can be concluded that the interatomic interactions decrease at the thinner films, indicating that the film structure is different for the thin and thick samples. This conclusion is confirmed by the XRD measurements presented in Sec. III B.

B. Structural properties

Information about the structural properties of pentacene films on glass substrates is obtained from the analysis of the XRD measurements. A typical example of XRD pattern of our samples is presented in Fig. 3(a). Two sets of peaks indexed as $(00l)$ and $(00l')$ are found which are assigned to reflections with different vertical periodicity. A strong preferential alignment with the $(00l)$ and $(00l')$ vectors perpendicular to the substrate are deduced. These results are typical for pentacene films and indicate the presence of two crystallographic phases.[30] The $(00l)$ peaks are assigned to the bulk phase,[35] which is observed in crystalline pentacene and usually dominates in thick films deposited at a substrate temperature higher than room temperature. The bulk phase is characterized by a vertical periodicity of 14.5 Å. The $(00l')$ peaks are assigned to another phase, which appears only in vapor deposited pentacene films.[30] This phase has a relatively higher vertical periodicity of 15.4 Å and is known as thin film phase.

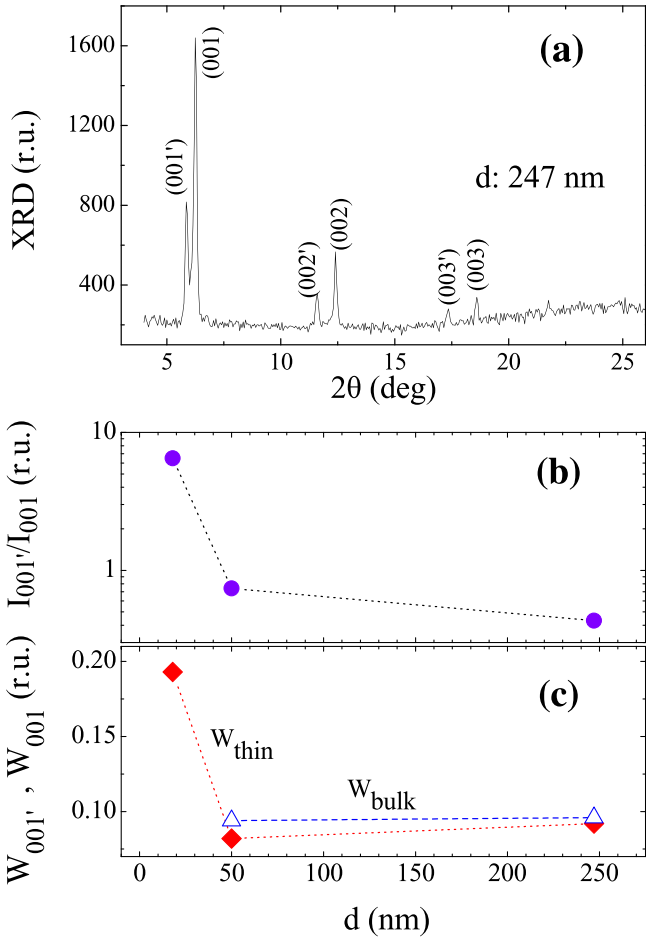

FIG. 3. (a) Typical XRD pattern of pentacene film ($d = 247$ nm). (b) Evolution with d of the ratio $I_{001'}/I_{001}$ of the intensity of the first order diffraction peak of the thin films phase to that of the bulk phase. (c) Evolution with d of the half width at half maxima $W_{001'}$ (diamonds) and W_{001} (triangles) of the first order diffraction peaks of thin film and bulk phases, respectively (broken lines serve as guide lines).

Fig. 3(b) demonstrates the evolution with thickness d of the ratio $I_{001'}/I_{001}$, which presents the intensity $I_{001'}$ of the first order diffraction peak of the thin film phase relative to that of the bulk phase I_{001}. Fig. 3(c) presents the evolution with d of the half width at half maxima, $W_{001'}$ and W_{001}, of the first order diffraction peaks of thin film and bulk phase, respectively. The peak $(001')$ corresponding to the thin film phase appears relatively broader in the thinner film ($d = 18$ nm) demonstrating the highest $W_{001'}$ width. This result suggests an enhanced structural disorder, which could be attributed to a mixture of different structures.[34] The thin film phase is induced by the substrate and usually dominates in films relatively thinner than a critical thickness, which mainly depends on the substrate temperature.[34,36,37] As it can be seen from Fig. 3(b), in our pentacene films, grown at room temperature on glass substrates, the thin film phase dominates for film thickness lower than 50 nm. Specifically, the thinnest sample of $d = 18$ nm practically consists of the thin film phase with negligible contribution from the bulk phase ($I_{001'}/I_{001} \gg 1$). Beyond d = 18 nm, the bulk phase is developing and starts to exceeds the thin film phase ($I_{001'}/I_{001} < 1$) as long as d is reaching 50 nm. For thicker films with $d > 50$ nm, the bulk phase predominates.

The relatively higher vertical periodicity of the thin film phase predominating in the thinnest films ($d = 18$ nm) is associated with relatively weaker intermolecular interactions.[37] This conclusion is compatible with the observed decrease of the Davidov splitting, ΔE, for the thinner films (see Fig. 2).

C. Photocurrent response

Fig. 4 presents the photocurrent i_p as a function of the photon energy for pentacene films of different thickness in comparison with the respective optical absorption spectra. For a better comparison, all the spectra were normalized to the respective first maximum around E_A. As it can be seen from Figs. 4(a) and 4(b), the i_p spectra of thinner films with $d = 18$ nm and $d = 50$ nm present maximum and minimum response at about the same photon energies for which the optical absorption presents maximum and minimum values, respectively. It can be concluded that the photocurrent can be excited by all the optical transitions involved in the main optical absorption bands centered at E_A, E_B, E_C, and E_D. Namely, the photocurrent response spectrum follows the respective optical absorption spectrum, demonstrating the so-called symbatic response. A similar behavior has been also reported by Gajewski *et al.*[25] and Fraboni *et al.*[38] from photoresponse measurements in pentacene films with a low thickness of 50 nm grown on SiO_2 substrate.

The photocurrent i_p spectra of the films with a thickness of $d = 80$ and 247 nm shown in Figs. 4(c) and 4(d), respectively, present almost featureless spectra. As it can be seen from these figures, the onset of the photocurrent is found at slightly lower energies than the respective onset of the optical absorption around 1.83 eV.

The photocurrent i_p spectrum of the thicker film of Fig. 4(e) with $d = 357$ nm exhibits pronounced maxima and minima which are "out-of-phase" from the respective maxima and minima of the absorption spectra. Namely, the maximum photocurrent appears at photon energies of minimum absorption coefficient and the minimum photocurrent appears for the photon energies of maximum absorption coefficient. The above antisymmetric behavior has been frequently observed in the photocurrent spectra of organic semiconductors and conjugated polymers and is known as antibatic response.[12,22,26,39–41] This behavior is also called inner filter effect as it eliminates the photocurrent response at high absorption. Antibatic response has been also observed in the photocurrent spectra of relatively thick tetracene and pentacene films.[42,43]

The evolution with the film thickness of the photoconductivity σ_p, measured at the fixed wavelength of 630 nm and normalized at the maximum value obtained at low d, is presented in Fig. 5 (solid circles). It can be seen that as a general trend σ_p increases with decreasing d.

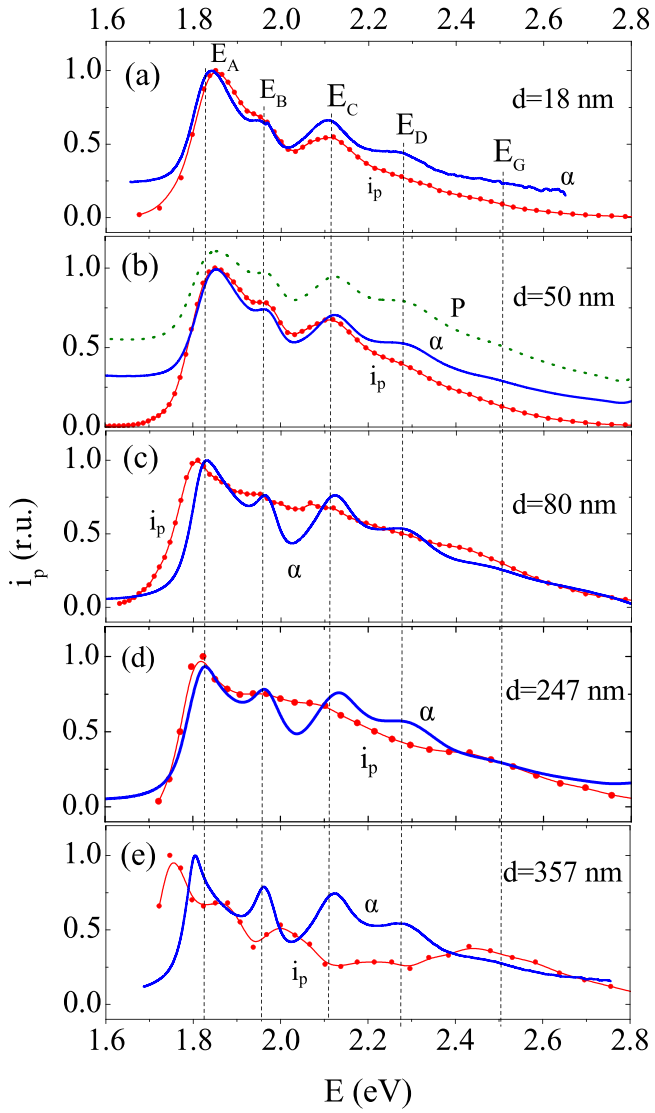

FIG. 4. As measured photocurrent i_p (solid circles and lines) and optical absorption α (solid lines) spectra normalized to the first maximum around E_A of pentacene films of $d = 18$ nm in (a), $d = 50$ nm in (b), $d = 80$ nm in (c), $d = 247$ nm in (d) and $d = 357$ nm in (e). P spectrum (dotted line) calculated from Eq. (3) for the α values of the sample with $d = 50$ nm is included in (b) for comparison.

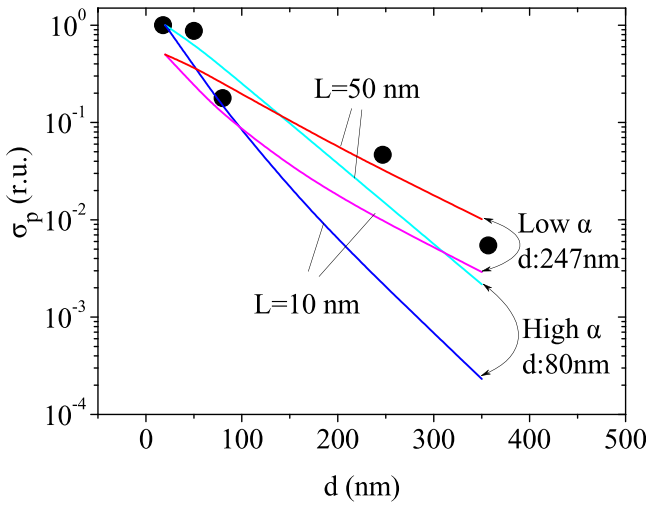

FIG. 5. Evolution with d of the photoconductivity σ_p normalized at the highest value at low d as obtained from the experiments (solid circles) and from the model simulations (solid lines) for a fixed wavelength of $\lambda = 630$ nm. The simulated σ_p were obtained by means of Eqs. (1)–(3) and (5) for the high and low α values of the samples with $d = 80$ and 247 nm, respectively, and for the indicated L values.

D. Normalized photocurrent response spectra

The spectra of Fig. 4 are the as measured photocurrent spectra, without correcting the wavelength dependence of the light flux, F_0, incident on the top surface of the films. For a more quantitative analysis, the i_p spectra are normalized to the light flux, F_{en}, entering the film which is calculated from $F_{en} = F_0(1 - R)$ by taking into account the measured reflection, R, from the top surface of the pentacene film. The normalized i_p/F_{en} spectra are presented in Fig. 6 in arbitrary units, in order to compare their spectral shape evolution with film thickness d. It is evident that the film thickness is an essential parameter for the spectral shape of the photocurrent response and this is probably related to the photocarrier generation mechanism.

As it can be seen from of Fig. 6, for the thinner films with $d = 18$ and 50 nm, which present the symbatic response, the photocurrent response spectra present structure with pronounced maxima around the photon energies E_A, E_B, E_C, and E_D of optical absorption peaks, which are usually attributed to excitonic transitions.

Pronounced maxima and minima are also found in the photocurrent response of thick sample with $d = 357$ nm in Fig. 6, but at the photon energies where the optical absorption presents minima and maxima, respectively, demonstrating clear antibatic response.

For films with an intermediate thickness of $d = 80$ nm and $d = 247$ nm, the i_p/F_{en} spectra appear practically featureless without pronounced peaks, demonstrating the transition from the symbatic to the antibatic response.

For films with $d > 50$ nm, the i_p/F_{en} becomes relatively low in the energy region of 1.7–2.2 eV where high optical absorption values are observed. In these films, the higher photocurrent response appears at the higher photon energies around $E_G \cong 2.5$ eV, where the optical absorption spectra present low absorption values and a weak shoulder. This weak shoulder could be attributed[22] to optical transitions which are not so apparent in the absorption spectrum, but they are pronounced in the photogeneration process of the thickest films. It could be attributed to photocarriers creation with the intrinsic process arising from optical transitions across the HOMO-LUMO gap, which is expected above 2.2 eV.[44]

The different behavior between the thin and thick films of the i_p/F_{en} spectra for energies lower than 2.5 eV indicates that the underlying photogeneration mechanism is sensitive to the film thickness. In this spectral region, the optical absorption coefficient presents strong energy dependence, which is a characteristic of excitonic transitions. However, a clear distinction between intrinsic and extrinsic photogeneration cannot be directly made from these results and a more detailed analysis is presented below.

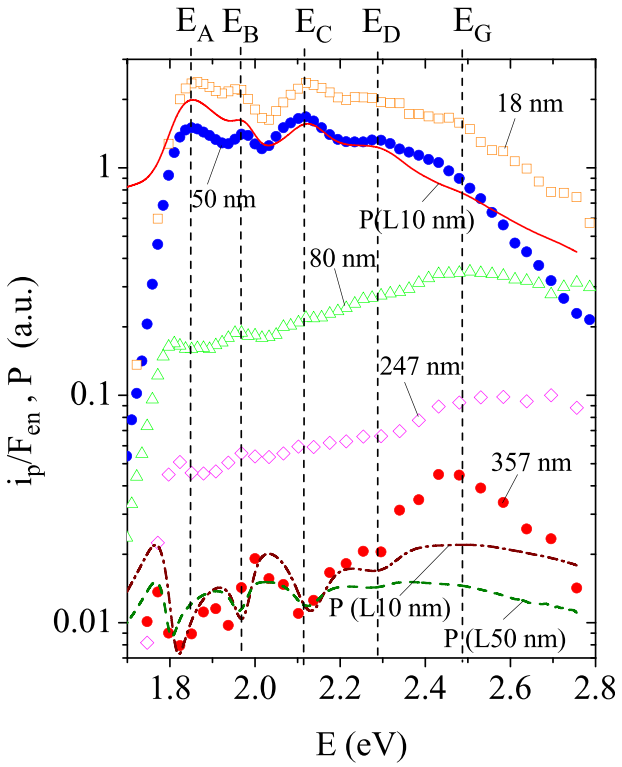

FIG. 6. Photocurrent response, i_p/F_{en}, in arbitrary units as a function of the photon energy for the films with the indicated thicknesses. The P spectra calculated by means of Eq. (5) for the sample of $d = 50$ nm assuming $L = 10$ nm (solid line) and for the thicker sample of $d = 357$ nm assuming $L = 10$ nm (dashed-dotted line) and $L = 50$ nm (dashed line) are included for comparison.

IV. ANALYSIS OF THE PHOTOCURRENT RESPONSE SPECTRA

A. Photocurrent generation and light penetration in the films

By assuming mobile charge carriers photogeneration throughout the entire film volume either directly from optical transitions across the HOMO-LUMO gap or from extrinsic process involving light created excitons which eventually dissociate, the photoconductivity, σ_p, is given by

$$\sigma_p = i_p \varepsilon l = \eta e \mu \tau G, \tag{1}$$

where ε is the electric field across the electrodes, $\mu\tau$ is the mobility lifetime product, e is the electronic charge, G is the absorbed photons per unit film volume, and η is the efficiency for mobile charge carrier creation. In the specific case of extrinsic photogeneration through excitons formation and dissociation, η is referred to the product $\eta = \eta_e \eta_g$ of the efficiency, η_e, of excitons creation and of the efficiency, η_g, of exciton dissociation into mobile charge carriers, which escape from geminate recombination. The parameter G is given by

$$G = \frac{F_0(1 - R)}{d} P. \tag{2}$$

where P is given by

$$P = \int_0^d \alpha \exp(-\alpha x) dx = 1 - exp(-\alpha d) \tag{3}$$

obtained assuming that mobile charge carrier creation is taking place from light absorption throughout the entire film thickness and considering that the number of the absorbed

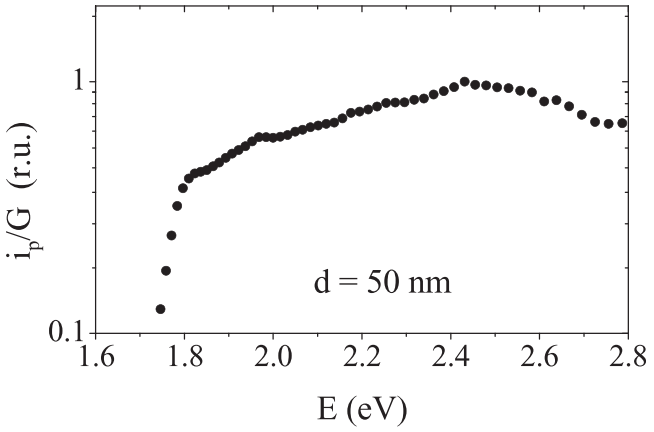

FIG. 7. Example of experimental i_p/G response of the photocurrent, i_p, normalized to the absorbed photon density, G (Eq. (2)), as a function of the photon energy for a thin film with $d = 50$ nm.

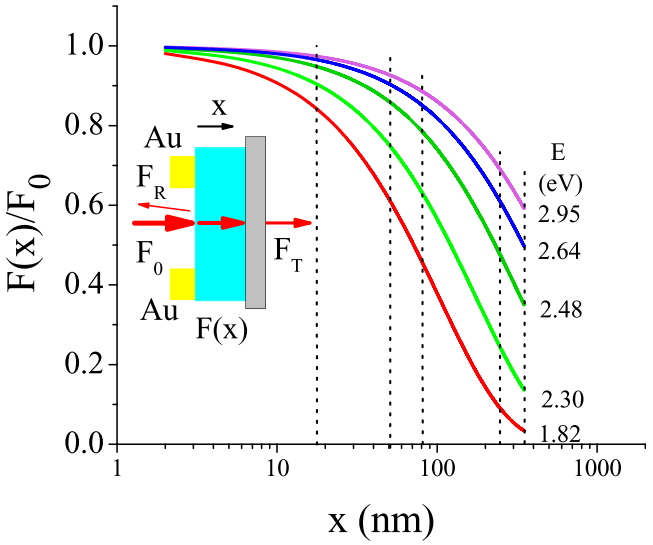

FIG. 8. Calculated relative magnitude $F(x)/F_0$ of the light flux penetrating in the films as a function of the distance, x, from the top illuminated free surface (see inset) for the indicated photon energies. Vertical dotted lines indicate the position of the substrate of the pentacene samples studied in this work.

photons in the range $x \rightarrow x + dx$ from the illuminated surface of the film is given by $F_0(1-R)\alpha\exp(-\alpha x)dx$. According to the above relation, P has a strong energy dependence with the photon energy due to the energy dependence of α. An example of such dependence is demonstrated in Fig. 4(b) (dotted line) for the film with $d = 50$ nm, where it can be seen that the P spectrum calculated from Eq. (3) roughly follows α spectrum. Since in the thin films ($d = 18$ and 50 nm), the energy dependence of i_p (Figs. 4(a) and 4(b)) and i_p/F_{en} (Fig. 6) follows the respective dependence of α, it can be concluded that the maxima and minima of the photocurrent spectra and the symbatic response are basically generated from the energy dependence of the parameter P of Eq. (3). This can be verified by normalizing the photocurrent to the generation rate, G, calculated from Eqs. (2) and (3). A typical example of normalized i_p/G spectrum of thin films is presented in Fig. 7 for the sample with $d = 50$ nm. This spectrum indicates a smooth decrease of the $\eta\mu\tau$ product with decreasing energy. Hence the maxima and minima of the i_p spectra practically originate from the variations of the parameter P according to Eq. (3) due to the strong energy dependence of the absorption coefficient.

By contrast, the antibatic photocurrent response of thick sample ($d = 357$ nm) of Figs. 4(e) and 6 is not compatible with the symbatic response of P spectra (see Fig. 4(b)) calculated from Eq. (3) assuming photocurrent generation by light absorption throughout the entire film volume. It can be concluded that in relatively thick films with $d > 50$ nm, the photocurrent is not efficiently generated from all the photons absorbed in the entire film volume.

A crucial factor in the photocurrent generation process is the fraction of the photon flux $F(x)$ penetrating the films. $F(x)$ strongly depends on the light absorption and the film thickness. Fig. 8 presents the profile of the variation of the relative photon flux, $F(x)/F_0$, as a function of the distance, x, from the top illuminated surface, as is calculated from $F(x) = F_0\exp(-\alpha x)$ for different photon energies of the incident illumination. As it can be seen from Fig. 8, the illumination of the higher photon energies, corresponding to low α values, is more uniformly absorbed throughout the entire film volume. By contrast, for lower photon energies, corresponding to the maxima of the α spectra, a strong light absorption takes place near the illuminated front surface of the pentacene films. Thus relatively fewer photons penetrate deeply in the bulk region of the thick films. The antibatic response is observed in thick films ($d = 357$ nm) where the higher photocurrent is generated by weakly absorbed light, which offers deep light penetration. This suggests that the photocurrent is mainly produced near the pentacene-substrate interface.[39,40,45] Appropriate mechanisms consistent with the above conclusion are presented in Secs. IV B and IV C.

B. Efficient carriers transport and/or photocarriers creation near the substrate interface

Efficient photocurrent for weakly absorbed light may be reproduced via two possible mechanisms which can be modelled by the same theoretical formalism. Specifically, near the pentacene-substrate interface, it can take place a better charge carriers transport and/or a pronounced charge carriers generation from efficient exciton dissociation.

The first mechanism can be based on the fact that a high mobility has been observed in OFETs consisting of only two layers of single thin film phase.[46] Based on this observation, it could be argued that the thin film phase developed near the substrate may be a high mobility phase. In fact, it is known that the transport of charge carriers in pentacene OFETs practically takes place near the insulating layer. Particularly, charge carriers transport is practically established within the first few monolayers of pentacene films.[47] Here, it is examined whether a possible better charge carriers transport near the pentacene-substrate interface may reproduce our experimental results. In this mechanism, the photocurrent can be generated either from mobile charge carrier creation directly from light absorption or through exciton dissociation.

The second mechanism involves extrinsic photogeneration via dissociation of light created excitons. As the light

created excitons are bound electron hole pairs, mobile charge carriers contributing to the photocurrent can result from the dissociation of these excitons by a more complicated process. Specifically, incident photons are absorbed in the samples within the light penetration depth and create excitons, which may diffuse. During this diffusion, the excitons have several possibilities to dissociate into charge carriers. This may be accomplished with the interaction of the excitons with deep gap states, such as impurities (like oxygen), defects, trapped charge at the interfaces, and electrodes.[22,48] Specifically, the electron of the bound electron-hole pair of the exciton near such a deep localized state may be captured. If the energy released from this capture process exceeds the exciton binding energy, the exciton dissociates and a hole (majority carrier) becomes available to contribute to the photocurrent. By assuming that exciton dissociation efficiently occurs within a narrow layer at the pentacene-substrate interface, it is examined below whether our results can be reproduced.

The above two possible mechanisms can be quantitatively modelled by means of Ghosh *et al.*[49] formalism, which was put forward earlier to account for the photocurrent response of organic diodes. This formalism can be applied assuming different diffusing species towards organic semiconductor interfaces where an efficient photocurrent generation occurs. These species may be light created mobile charge carriers,[49] for the case of the first mechanism, which involves a better transport of the charge carriers near the substrate. Alternatively, the diffusing species may be light created excitons,[39] for the case of the second mechanism which involves photocurrent generation from efficient dissociation of excitons near the pentacene-substrate interface.

According to the formalism of Ghosh *et al.*[49] the number of the above light created species (mobile charge carriers or excitons), which are created in the range $x \rightarrow x + dx$ from the illuminated surface of the film, is proportional to $F_0(1-R)\alpha\exp(-\alpha x)dx$. As long as a better carriers transport and/or efficient exciton dissociation take place within a narrow pentacene layer of thickness l_b near the pentacene-substrate interface, then the light created species may diffuse to the narrow layer with a diffusion probability of $\exp(-(d-l_b-x)/L)$, where L is the diffusion length of the species.

Therefore, the total number, N, of the light created species at the narrow layer is proportional to

$$N = \int_0^{d-l_b} F_0(1-R)\alpha\exp(-\alpha x)\exp\left(\frac{l_b+x-d}{L}\right)dx + \int_{d-l_b}^{d} F_0(1-R)\alpha\exp(-\alpha x)dx, \quad (4)$$

where the first integral represents the number of the species which are created in the bulk of the film and diffuse at the narrow layer and the second integral represents the number of species created at the narrow layer. In fact, the total number of the mobile charge carriers is proportional to N, which can be obtained after integration of Eq. (4). This way, the parameter P appearing in Eq. (2) becomes

$$P = \frac{\alpha}{\alpha - 1/L}\left[\exp\left(-\frac{d-l_b}{L}\right) - (\exp(-\alpha(d-L))\right] + \exp(-\alpha d)(\exp(-\alpha l_b) - 1). \quad (5)$$

The above equation is used to simulate the parameter P, in order to explore the effect of the sample thickness, diffusion length, L, and optical absorption coefficient, α, on the spectral shape of P and eventually on the photocurrent response spectra. The thickness l_b of the narrow layer was taken much lower than the thickness of the thicker samples in order to reproduce the antibatic response. A fixed $l_b = 20$ nm was introduced in the simulations which corresponds to the thickness of the samples practically consisting of the thin film phase according to XRD results. This is a reasonable choice for l_b as long as the thin film phase is the high mobility phase promoting transport of the charge carriers at the narrow layer. Alternatively, the enhanced structural disorder of the thin film phase, concluded from the XRD results, may facilitate exciton dissociation within $l_b = 20$ nm. These two possibilities will be further discussed in Sec. V.

Typical examples of the P spectra simulated by means of Eq. (5) are presented in Fig. 9. It is found that the absolute magnitude and the spectral shape of the P spectra strongly depend on the absolute magnitude of the absorption coefficient. Specifically, Figs. 9(a) and 9(b) present P spectra calculated by introducing the relatively high optical absorption values experimentally obtained from the sample with $d = 80$ nm (Fig. 1). Figs. 9(c) and 9(d) present P spectra calculated by introducing the relatively low optical absorption values experimentally obtained from the sample with $d = 247$ nm (Fig. 1). All the P spectra of Fig. 9 present a qualitatively similar behavior with that of the experimental photocurrent response. Namely, upon increasing d, a transition from the symbatic to the antibatic response is observed around a critical thickness d_{cr}. This critical thickness is found at significantly lower d for relatively higher absolute optical absorption values (compare Figs. 9(a) and 9(b) with Figs. 9(c) and 9(d)). A relatively smaller shift of the d_{cr} to lower values is obtained upon decreasing L from 50 nm (Figs. 9(a) and 9(c)) to 10 nm (Figs. 9(b) and 9(d)). The amplitude difference between the successive maxima and minima of the antibatic response, obtained within the spectral region extending from 1.7 to 2.2 eV for $d > d_{cr}$, is less pronounced as long as relatively lower optical absorption coefficient values are introduced in the simulations (compare Figs. 9(a) and 9(b) with Figs. 9(c) and 9(d)).

C. High surface recombination

An alternative possible mechanism, which may give rise to antibatic photoresponse, involves a high recombination rate near the illuminated top surface of the pentacene film. It has been originally proposed by DeVore[50] to model the peak of the photocurrent response near the absorption edge of inorganic semiconductors. Lee *et al.*[51] and Harrison *et al.*[22] applied this model to explain the photocurrent response of organic semiconductors. According to this model in relatively thick samples having thickness of approximately the

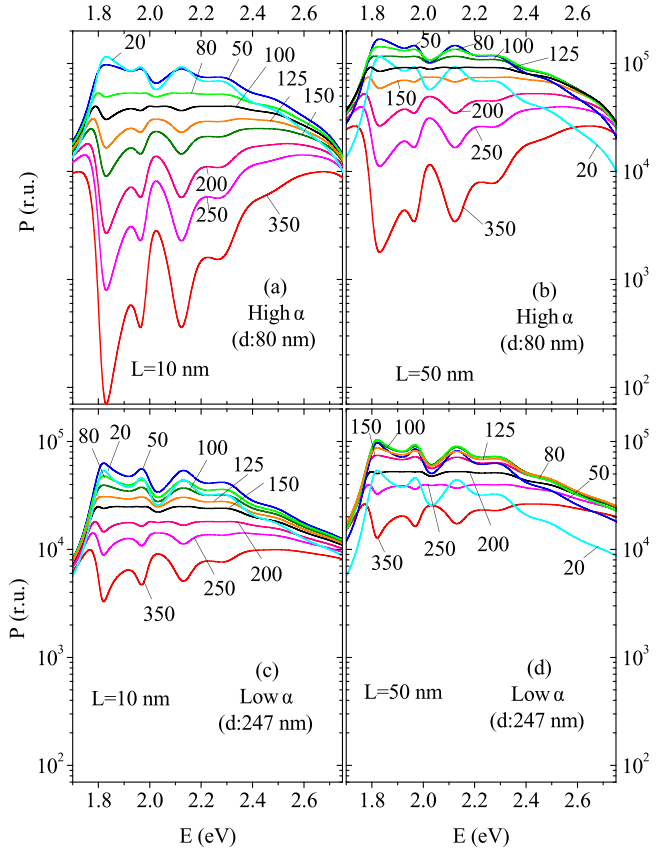

FIG. 9. Evolution with the thickness d of the P spectrum calculated from Eq. (5) for a fixed $l_b = 20$ nm by introducing the relatively high ((a) and (b)) and low ((c) and (d)) optical absorption coefficient values experimentally obtained from the films with $d = 80$ nm and $d = 247$ nm, respectively, for $L = 10$ nm ((a) and (c)) and $L = 50$ nm ((b) and (d)).

same order of magnitude with the light penetration depth or higher, a higher surface recombination rate compared to the bulk recombination rate may produce antibatic response.[22] By contrast, a low recombination rate produces symbatic response.

Specifically, a high recombination rate may take place near the free illuminated surface where a relatively high density of mobile charge carrier creation takes place, especially for the strongly absorbed light. In this region, a significant fraction of the created photocarriers may be lost from a high recombination rate due to a possible high surface states density resulting in a relatively low photocurrent response. By contrast, a weakly absorbed light is more uniformly absorbed in thick films (see Fig. 8). As a result, a relatively large fraction of the photocarriers are created far from the illuminated surface so that they have a better chance to survive from surface recombination giving rise to a relatively higher photocurrent and antibatic response.

The quantitative analysis proposed by DeVore includes a thin film photoconductor with electrodes in coplanar configuration illuminated from the free surface. At each point of the sample, the generation of mobile charge carriers is taken proportional to the absorption at that point. Since there is a gradient in the carrier density, the charge carriers diffuse with a diffusion constant, D, and diffusion length, L. The carriers created at certain depths from the illuminated surface in the bulk of the film undergo recombination. The carriers that diffuse to the top illuminated surface recombine with a rate which may be represented by a surface recombination velocity, S, which is the product of the carrier velocity and the recombination probability that occurs when a carrier reaches the surface. Based on the above assumptions, DeVore solved the rate equation and derived the expression of the spectral dependence of the photoconductivity σ_p as

$$\sigma_p = \frac{1-\exp(-\alpha d)}{1+(SL/D)coth(1/(2L))} \times \left[1+\frac{(S/D)((1/L)coth(d/(2L))-\alpha coth(\alpha d/2)}{1/L^2-\alpha^2}\right]. \quad (6)$$

Fig. 10 presents examples of the spectral response σ_p calculated from Eq. (6) for various film thickness by assuming the relatively high values of $L = 100$ nm and $S = 100$ m/s. For the diffusion constant, it is taken $D = 5 \times 10^{-4}$ cm^2/s, as deduced from ultrafast transient absorption measurements.[52] It can be seen that a transition from the symbatic to antibatic response at a critical thickness, d_{cr}, is reproduced. d_{cr} is around 300 nm by introducing in the simulation the relatively high optical absorption values experimentally obtained from the film with $d = 80$ nm. d_{cr} shifts to even higher values upon introducing relatively lower optical absorption values (not shown). It is also found that by introducing lower values for the L and S parameters than those introduced above, the transition to antibatic response appears at much higher film thickness than $d = 300$ nm. It is worthy to mention that the above model anticipates a strong decrease of the photoconductivity upon decreasing d, due to the enhanced contribution from a high surface recombination rate.

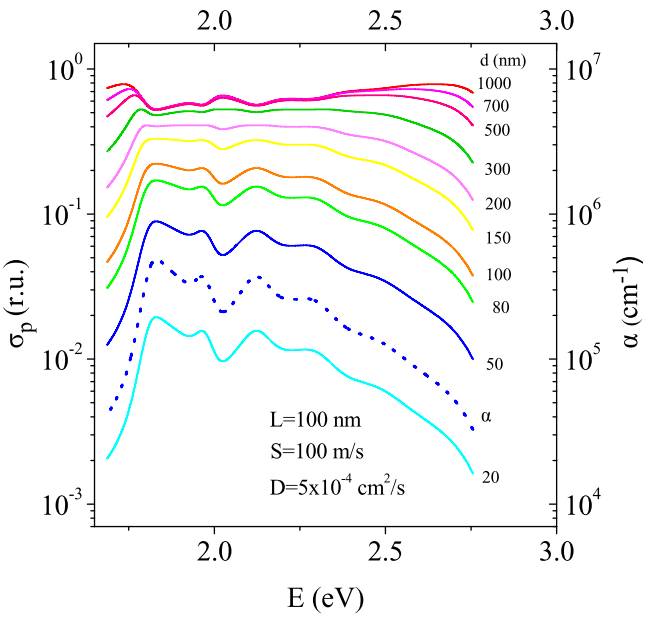

FIG. 10. Evolution with the film thickness of the photoconductivity response (solid lines and left axis) as calculated according to the model of DeVore (Eq. (6)) for the relatively higher optical absorption (dotted line and right axis) from the sample with $d = 80$ nm.

V. DISCUSSION

Our experimental results indicate that the optical, structural, and photoelectric properties of pentacene films depend on their thickness. In this section, all these observations are combined in order to get an insight into the photocurrent generation process by means of the different models of photoresponse presented in the previous sections. Although qualitatively all the examined models reproduce the symbatic to antibatic transition upon increasing d, the quantitative predictions of these models differ. Specifically, the model of a high surface recombination of DeVore predicts a strong decrease of the photoconductivity with decreasing film thickness. This prediction is opposite from the observed increase of the photoconductivity with decreasing d (see Fig. 5) making the Devore's model unfavorable to explain our results. Besides this, the above model predicts the symbatic to antibatic transition at relatively high critical thickness, d_{cr}. The lowest d_{cr} which is reproduced by this model is $d_{cr} \cong 300$ nm, which is much higher than the lowest one found experimentally at 80 nm.

The basic characteristics of the experimental photocurrent response spectra are reproduced assuming the microscopic mechanisms, which are based on a better transport and/or efficient exciton dissociation near the pentacene-substrate interface, as it was demonstrated in Sec. IV. According to this modelling, the calculated P parameter from Eq. (5) systematically increases with decreasing d (see Fig. 9). Such an increase of P produces through Eq. (1) an increase in the photoconductivity with decreasing d, similar with that experimentally observed, as is illustrated in Fig. 5 (solid lines). Moreover, according to Eqs. (1) and (2), the energy dependence of the photocurrent response (i_p/F_{en}) is expected to reflect that of the $\eta\mu\tau P$ product. A smooth energy dependence for the $\eta\mu\tau$ product was deduced from the analysis of the photoresponse of the thin films (see Fig. 7). By assuming a similar dependence for thicker samples, the energy dependence of the $\eta\mu\tau P$ product is expected to more likely governed by the P parameter (Eq. (2)). Therefore, the spectral shape of the normalized i_p/F_{en} spectra can be directly compared with that of the calculated P spectra. Indeed, it is remarkable that the essential features of the experimental normalized i_p/F_{en} spectra of Fig. 6 and their evolution obtained upon changing d can be reproduced with the simulated P spectra of Fig. 9.

Specifically, the simulated P spectra reproduce the symbatic and antibatic response of the experimental i_p/F_{en} spectra observed for low d (18 and 50 nm) and high d (357 nm), respectively. For film thickness around a narrow range of a critical thickness, d_{cr}, the spectral shape of P spectra in Fig. 9 practically become featureless demonstrating the symbatic to antibatic transition. Featureless i_p/F_{en} spectra indicating this transition are experimentally found as well, but in the samples with very different thickness of $d = 80$ and $d = 247$ nm. According to our simulations of Fig. 9, d_{cr} mainly depends on the absolute magnitude of the introduced optical absorption values, while a relatively smaller effect in d_{cr} was found from changes in the diffusion length, L. Hence the fact that the featureless i_p/F_{en} spectra manifesting the symbatic to antibatic transition appears in samples with very different thickness can be reconciled with the different magnitude of the optical absorption observed between the thinner and thicker samples.

Indeed, by introducing in the simulations, the relatively higher experimental optical absorption values from the sample of $d = 80$ nm, a featureless P spectrum is observed, indicating the symbatic to antibatic transition, at relatively low d_{cr} (see Figs. 9(a) and 9(b)). For L of the order of 10 nm, this transition is observed around $d = 80$ nm (see Fig. 9(a)), reproducing the respective transition of the experimental spectrum with $d = 80$ nm (see Fig. 6). Fig. 11(a) presents a more detailed evolution with L of the P spectra, calculated for the absorption coefficient of the sample of $d = 80$ nm. From this figure, it can be confirmed that the symbatic to antibatic transition is observed at relatively low L around 10 nm.

Similarly, by introducing in the simulations the relatively lower optical absorption values from the thicker sample of $d = 247$ nm, the symbatic to antibatic transition is observed in the P spectra at relatively higher thickness (see Figs. 9(c) and 9(d)). For a relatively high L of the order of 50 nm, this transition is observed around $d = 200$ nm (see Fig. 9(d)), which is close to the respective experimental

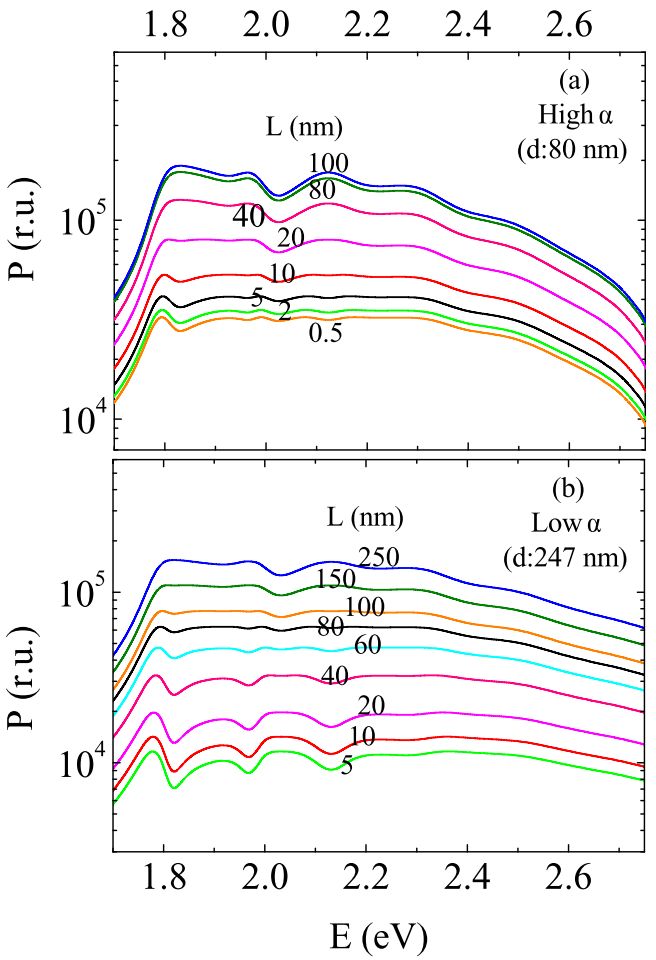

FIG. 11. Detailed evolution with the diffusion length L of the P spectra calculated from Eq. (5) for the relatively high (a) and low (b) optical absorption coefficient values experimentally obtained from the films with $d = 80$ nm and $d = 247$ nm, respectively.

transition observed for $d = 247$ nm (see Fig. 6). From a more detailed evolution with L of the P spectra calculated for the absorption of the sample of $d = 247$ nm presented in Fig. 11(b), the symbatic to antibatic transition more accurately appears for L around 80 nm. This way, an estimation of L is obtained which suggests an increase of the L from 10 nm in the thin films to 80 nm for the thicker films.

Our simulations of Fig. 9 indicate that the amplitude difference between the successive maxima and minima appearing in the P spectra of thick samples with antibatic response strongly depends on the absolute magnitude of the optical absorption values. This amplitude appears significantly smaller for the relatively lower optical absorption values of the thick samples, which demonstrate the antibatic response, so that the P spectra are very similar with the respective photoresponse experimental spectra. More specifically, examples of P spectra calculated for $d = 357$ nm by assuming $L = 10$ nm (dashed-dotted line) and 50 nm (dashed line) and introducing the respective optical absorption values from the thick sample of $d = 357$ nm are included in Fig. 6 (broken lines) for direct comparison. It can be seen that the antibatic response of the experimental i_p/F_{en} spectrum for energies lower than 2.2 eV is satisfactorily reproduced by the simulation, especially with the relatively higher $L = 50$ nm (dashed line). Nevertheless, the maximum appearing around $E_G \cong 2.5$ eV of the experimental spectrum appears more pronounced than that of the calculated P spectra. As mentioned above, this could be attributed to direct photocarrier generation across the HOMO-LUMO gap at the higher photon energy spectral region ($E > 2.2$ eV) with relatively higher probability.

Upon decreasing d below d_{cr}, the response of the calculated and experimental spectra at lower photon energies ($E < 2.5$ eV) increases presenting similar maxima with those of the optical absorption spectra. This is due to the low thickness for which the light beam appears more uniformly absorbed throughout the entire film volume, even for highly absorbed photons (see Fig. 8). In this case, the P spectra practically follow the respective photocurrent response spectra. This is demonstrated in Fig. 6 with an example of P spectrum of $d = 50$ nm (solid line) calculated by introducing in the calculation the optical absorption of the sample with the same thickness and assuming $L = 10$ nm. Note that a higher $L = 50$ nm does not significantly affect the spectral shape of the calculated P spectra of low thickness $d = 18$ and 50 nm (see Figs. 9(a) and 9(b)).

The above analysis showed that the two proposed microscopic mechanisms examined by means of Ghosh *et al.*[49] formalism appear favorable to explain the experimental results. The XRD results could be helpful to make a distinction between the above two mechanisms.

Specifically, it is examined whether the results of XRD can support a better charge carriers transport within a pentacene narrow layer near the substrate. According to the XRD results, during the early stage of pentacene deposition, the substrate induced thin film phase is developed. The thin film phase has a relatively higher vertical periodicity from a more perpendicular alignment of the pentacene molecules to the substrate which is associated to relatively weaker interatomic interactions. This is also supported from the relatively lower Davidov splitting ($\Delta E \cong 0.1$) of the thinner films (see Fig. 2). By contrast, the bulk phase, dominating in thick films, is characterized by a relatively lower vertical periodicity and an increased Davidov splitting ($\Delta E \cong 0.15$). This is associated to a stronger coupling in the intermolecular π-electron system of pentacene molecules within the crystals which promotes charge carriers transport. As a result, an inferior charge carriers transport is expected for the thin film phase dominating near the pentacene-substrate interface compared to that of the bulk phase.[37] Therefore, the XRD film structural properties cannot support a better charge carriers transport near the pentacene-substrate interface.

By contrast, the XRD patterns provide support to the second mechanism of efficient exciton dissociation near the pentacene-substrate interface. As mentioned above, for the sample with $d = 18$ nm, the broad first diffraction peak $(001')$, which dominates XRD pattern and assigned to the thin film phase, indicates an inhomogeneous broadening of the local environment and a mixture of different structures. It can be concluded that the first approximately 20 nm of the deposited pentacene films consists of a narrow layer of thin film phase close to the substrate with an enhanced structural disorder, which may facilitate efficient exciton dissociation. Additional centers which facilitate exciton dissociation near the substrate may be impurities, like water or oxygen, which could be adsorbed during the exposure of the substrates in the ambient air. If the above are combined with the possible formation of interfacial dipoles, which give rise to local electric fields that can trigger charge separation over long distances, then the mechanism of efficient exciton dissociation near the pentacene-substrate interface appears favorable as the predominant photocarriers creation mechanism. This interpretation is further supported from the fact that the estimated L in the region of 10 to 80 nm deduced from the model simulations is reasonable for the diffusion length of excitons in pentacene.[53,54] As long as the photoresponse spectra within 1.7-2.2 eV is successfully reproduced by involving exciton dissociation near the substrate, it can be concluded that the extrinsic photogeneration is involved throughout the above spectral energy region.

VI. CONCLUSIONS

The analysis of the photocurrent response spectra suggests that the photocarriers may be practically generated by light absorption within the entire film volume only for samples having thickness of the order of 50 nm and lower. In this case, the photoresponse demonstrates symbatic response. For thicker samples, a relatively higher photocurrent is observed for deeply penetrating light near the pentacene-substrate interface demonstrating antibatic response. The photocurrent response is found not compatible with an enhanced surface recombination rate. The spectral shape and the evolution with the film thickness of the experimental photocurrent response can be reproduced by a model which assumes that near the pentacene-substrate interface preferably takes place either a better transport of the photocarriers and/or efficient exciton dissociation. The simulations show that the spectral shape of the experimental spectra and the symbatic to

antibatic transition depend not only on the film thickness but also on the absolute magnitude of the optical absorption and the diffusion length of the light created species.

The structural properties deduced from the XRD patterns revealed the growth of a thin film phase within about 18 nm from the substrate. The reduced intermolecular interactions of the thin film phase cannot support a better charge carriers transport near the pentacene-substrate interface. In contrast, the disordered thin film phase, which dominates within a thin layer of 18 nm of pentacene grown close to the substrate, along with the possible existence of adsorbed impurities and interfacial dipoles, may facilitate dissociation of excitons and provide support to the extrinsic photogeneration process near the pentacene-substrate interface. Namely, the excitons created in the bulk region of the films by absorption of photons in the region of 1.7–2.2 eV, diffuse to a narrow layer of about 20 nm at the pentacene-substrate interface with a diffusion length, L, of the order of 10 to 80 nm. At this interface, the diffusing excitons along with those that are created in the narrow layer dissociate providing mobile charge carriers contributing to the photocurrent.

ACKNOWLEDGMENTS

S.G. was financially supported by the project "C. Carathéodory" University of Patras and A.G. was financially supported by the state scholarships foundation (IKY).

[1]G. Horowitz, Adv. Mater. **10**, 365 (1998).
[2]R. Benchabane, M. Gaoudi, and G. Guillaud, Synth. Met. **67**, 231 (1994).
[3]G. Guillaud, J. Simon, and J. P. Germain, Coord. Chem. Rev. **178–180**, 1433 (1998).
[4]J. Y. Kim, T. Z. Shin, and M. K. Yang, J. Elec. Eng. Technol. **2**, 408 (2007).
[5]D. Xie, W. Pan, Y. D. Jiang, and Y. R. Li, Mater. Lett. **57**, 2395 (2003).
[6]C. D. Dimitrakopoulos and P. R. L. Malenfant, Adv. Mater. **14**, 99 (1990).
[7]M. Kitamura and Y. Arakawa, J. Phys.: Condens. Matter **20**, 184011 (2008).
[8]H. Klauk, M. Halik, U. Zschieschang, G. Schmid, W. Radik, and W. Weber, J. Appl. Phys. **92**, 5259 (2002).
[9]T. W. Keley, L. D. Boardman, T. D. Dumbar, D. V. Muyres, M. J. Pellerie, and T. P. Smith, J. Phys. Chem. B **107**, 5877 (2003).
[10]S. Lee, B. Koo, J. Shim, E. Lee, H. Park, and H. Kim, Appl. Phys. Lett. **88**, 162109 (2006).
[11]D. Knipp, R. A. Street, A. Volkel, and J. Ho, J. Appl. Phys. **93**, 347 (2002).
[12]Y. Noh and D. Kim. Solid-State Electron. **51**, 1052 (2007).
[13]A. Rao, M. W. B. Wilso, J. M. Hodgkiss, S. Albert-Seifried, H. Bassler, and R. H. Friend, J. Am. Chem Soc. **132**, 12698 (2010).
[14]A. K. Pandey and J. M. Nunzi, Appl. Phys. Lett. **89**, 213506 (2006).
[15]J. T. Mebeck and G. G. Malliaras, Anal. Bional. Chem. **384**, 343 (2006).
[16]Y. Y. Noh, J. Ghim, S. J. Kang, K. J. Baeg, and D. Y. Kim, J. Appl. Phys. **100**, 094501 (2006).
[17]C. S. Suchand Sangeeth, P. Stadler, S. Schaur, N. S. Sariciftci, and R. Menon, J. Appl. Phys. **108**, 113703 (2010).
[18]L. Sebastian and G. Weiser, Chem. Phys. **61**, 125 (1981).
[19]M. Grobosch, R. Schuster, T. Pichler, and M. Knupfer, Phys. Rev. B **74**, 152202 (2006).
[20]R. Schuster, M. Knupfer, and H. Berger, Phys. Rev. Lett. B **98**, 037402 (2007).
[21]R. G. Kepler, J. M. Zeigler, L. A. Harrah, and S. R. Kurtz, Phys. Rev. B **35**, 2818 (1987).
[22]M. G. Harrison, J. Gruner, and G. C. W. Spencer, Phys. Rev. B **55**, 7831 (1997).
[23]J. Lee, D. K. Hwang, C. H. Park, S. S. Kim, and S. Im, Thin Solid Films **451–452**, 12 (2004).
[24]B. Fraboni, A. Matteouci, and A. Cavallini, Appl. Phys. Lett. **89**, 222112 (2006).
[25]W. Gajewski, M. Hoth, F. Buth, B. NIckel, M. Stutzmann, and J. A. Garrido, Phys. Rev. B 80, 235311 (2009).
[26]J. Puigdollers, C. Voz, A. Orpella, I. Martin, M. Vetter, and R. Alcubilla, Thin Solid Films **427**, 367 (2003).
[27]E. A. Silinsh, *Organic Molecular Crystals* (Springer, Berlin, 1980).
[28]F. Amy, C. Chan, and A. Kahn, Org. Electron. **6**, 85 (2005).
[29]J. Lee, S. S. Kim, K. Kim, J. H. Kim, and S. Im, Appl. Phys. Lett. **84**, 1701 (2004).
[30]C. D. Dimitrakopoulos, A. R. Brown, and A. Pomp, J. Appl. Phys. **80**, 2501 (1996).
[31]O. Ostroverkhova, S. Shcherbyna, D. G. Cooke, R. F. Egerton, and F. A. Hegmann, J. Appl. Phys. **98**, 033701 (2005).
[32]R. He, N. G. Tassi, G. B. Blanchet, and A. Pinczuk, Appl. Phys. Lett. **87**, 103107 (2005).
[33]R. Hesse, W. Hofberger, and H. Bassler, Chem. Phys. **61**, 125 (1981).
[34]T. Jentzsch, H. J. Juepner, K. W. Brzezinka, and A. Lau, Thin Solids Films **315**, 273 (1998).
[35]R. B. Campbell and J. M. Robertson, Acta Crystallogr. **15**, 289 (1962).
[36]I. P. M. Bouchoms, W. A. Schoonveld, J. Vrijmoeth, and T. M. Klapwijk, Synth. Met. **104**, 175 (1999).
[37]H. L. Cheng, Y. S. Mai, W. Y. Chou, L. B. Chang, and X. W. Liang, Adv. Funct. Mater. **17**, 3639 (2007).
[38]B. Fraboni, A. Scida, A. Cavallini, P. Cosseddu, A. Bonfiglio, S. Mitta, and M. Nastasi, Appl. Phys. Lett. **96**, 163302 (2010).
[39]A. Ghosh and T. Feng, J. Appl. Phys. **49**, 5982 (1978).
[40]N. Karl, A. Bauer, J. Holzapfer, J. Marktanner, M. Mobus, and F. Stolzle, Mol. Cryst. Liq. Cryst. **252**, 243 (1994).
[41]F. Feller and A. P. Monkman, Appl. Phys. Lett. **76**, 664 (2000).
[42]D. Kotowski, B. Kutrzeba-Kotowska, M. Obarowska, R. Signerski, and J. Godlewski, Org. Electron. **6**, 193 (2005).
[43]M. Obarowska, D. Kotowski, K. Porath, J. Signerski, and J. Godlewski, Org. Electron. **6**, 193 (2005).
[44]D. V. Lang, X. Chi, T. Siegrist, A. M. Sergent, and A. P. Ramirez, Phys. Rev. Lett. **93**, 086802 (2004).
[45]C. Voz, J. Puigdollers, I. Martin, D. Munoz, A. Orpella, M. Vetter, and R. Alcubilla, Sol. Energy. Mater. Sol. Cells **8–10**, 940 (1972).
[46]Y. Y. Lin, D. J. Gudlach, S. F. Nelson, and T. N. Jackson, IEEE Electron Device Lett. **18**, 12 (1997).
[47]A. S. Shehu, S. D. Quiroga, P. D' Angelo, C. Albonetti, F. Borgatti, M. Murgia, A. Scorzoni, P. Stoliar, and F. Biscarini, Phys. Rev. Lett. **104**, 246602 (2010).
[48]E. A. Silinsh, A. I. Belkind, D. R. Balode, A. J. Biseniece, V. V. Crechov, L. F. Taure, M. V. Kurik, J. I. Vertzymacha, and I. Bok, Phys. Status Solidi **25**, 339 (1974).
[49]A. Ghosh, D. L. Morel, T. Feng, R. F. Shaw, and C. A. Rowe, Jr., J. Appl. Phys. **45**, 230 (1974).
[50]H. B. DeVore, Phys. Rev. **102**, 86 (1956).
[51]C. H. Lee, G. Yu, and A. J. Heeger, Phys. Rev. B **47**, 15543 (1993).
[52]H. Marcinak, M. Fiebig, M. Huth, S. Sciefer, B. Nickel, F. Selmaier, and S. Lochbrunner, Phys. Rev. Lett. **99**, 176402 (2007).
[53]S. Yoo, W. J. Potscavage, Jr., B. Domercq, S. Han, T. Li, S. C. Jones R. Szoszkiewicz, D. Levi, E. Riedo, S. R. Marder, and B. Kippelen Solid-State Electron. **51**, 1367 (2007).
[54]B. Park, P. Paoprasert, P. Goplan, Y. W. Wang, Y. S. Mai, and F. C. Tang, Adv. Funct. Mater. **18**, 285 (2008).